Supporting Information

Expanding the Zinc Precursor Toolbox: A Comparative Study of Precursors for Thermal ALD of ZnO Thin Films

Jorit Obenlüneschloß,[1] Rajesh Pathak,[2] Vepa Rozyyev,[2] Anil U. Mane,[2] Thomas Gemming,[3] Detlef Rogalla,[4] Jeffrey W. Elam,[2 *] and Anjana Devi[1, 3, 5, 6 *]

[1]Inorganic Materials Chemistry, Ruhr University Bochum, 44801 Bochum, Germany
[2]Applied Materials Division, Argonne National Laboratory, Chicago, Illinois 60637, United States
[3]Leibniz Institute for Solid State and Materials Research, IFW Dresden, 01069 Dresden, Germany
[4]RUBION, Ruhr University Bochum, Universitätsstr. 150, 44801 Bochum, Germany
[5]Chair of Materials Chemistry, TU Dresden, 01069 Dresden, Germany
[6]Fraunhofer Institute for Microelectronic Circuits and Systems, IMS, 47057 Duisburg, Germany
*Corresponding author: a.devi@ifw-dresden.de and jelam@anl.gov

Table of Contents

Precursor Synthesis

Precursor synthesis and purification were performed under argon using standard Schlenk techniques. THF, diethyl ether, and n-hexane were purified and dried with an MBraun solvent purification system (MBraun SPS). All the compounds, including $ZnCl_2$ (abcr, 98%, anhydrous) and diethyl zinc used for synthesis (Sigma Aldrich, DEZ, $Zn(Et)_2$ (>52 wt% Zn) were stored, handled, and prepared for analysis under an argon atmosphere (Air Liquide, 99.999%) in a glove box (MBraun, Labmaster 120). For precursor analysis, ^1H nuclear magnetic resonance (NMR) spectra were recorded on a Bruker DPS 300 spectrometer. All spectra were referenced to internal solvent proton signals. The recorded NMR spectra were analyzed using MestReNova software.

Bis-(N,N-dimethylamino)propyl zinc(II), $Zn(DMP)_2$:

$Zn(DMP)_2$ was prepared as previously described by Mai *et al.*[1] A solution of $ZnCl_2$ (1 equivalent) in THF was cooled to 0 °C and added dropwise to a cooled (0 °C) solution of 3-(N,N-dimethylamino)propyl magnesium chloride (2 equivalents) in THF that was synthesized as described in the literature (Scheme S1).[2] The resulting suspension was allowed to warm, refluxed overnight at 80 °C, and then stirred at room temperature. The THF was removed under reduced pressure, and the colorless solid was extracted in hexane. The suspension was filtered through a Celite-padded filter, and the volatiles were removed under reduced pressure. The colorless solid was purified by sublimation at 60 °C to obtain spectroscopically pure $Zn(DMP)_2$ (yield: 51%).

^1H NMR (400 MHz, Benzene-d6) δ [ppm] = 2.06–1.99 (4H, m, $[(CH_3)_2N\underline{CH_2}CH_2\underline{CH_2}Zn]$), 1.98–1.90 (m, 4H, $[(CH_3)_2N\underline{CH_2}CH_2\underline{CH_2}Zn]$), 1.88 (s, 12H, $[(CH_3)_2N\underline{CH_2}CH_2\underline{CH_2}Zn]$), 0.32 (4H, t, $[(CH_3)_2NCH_2\underline{CH_2}CH_2Zn]$).

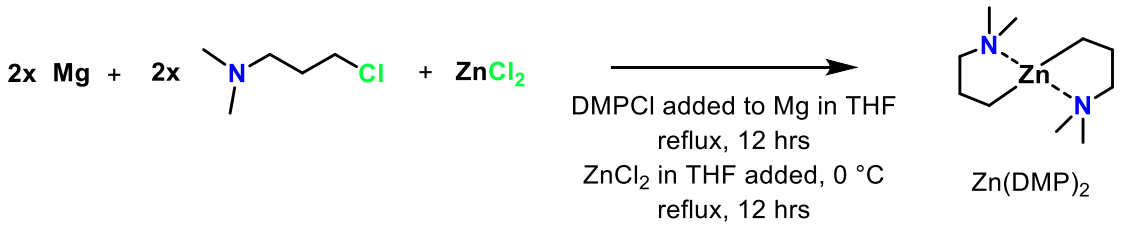

Scheme S1: Synthesis of $Zn(DMP)_2$.

Bis(N-(2′-ethoxyethyl)-2-penten-2-on-4-iminate) zinc(II), $Zn(EEKI)_2$:

The protonated free ligand H(EEKI) was prepared according to the literature-known procedure, and the synthesis of $Zn(EEKI)_2$ followed the published protocol.[3] To a stirred solution of diethylzinc in hexane, two equivalents of N-(2′-ethoxyethyl)-2-penten-2-ol-4-imine [H(EEKI)] were added via a syringe at −20 °C (Scheme S2). The solution was warmed to room temperature and stirring continued overnight. The solution was concentrated, and the product was crystallized at −30 °C. Pale yellow needle-like crystals were isolated by decanting the remaining solvent. The crystals were then washed with cold hexane and dried under vacuum (Yield: 93.4%).

^{1}H NMR (400 MHz, Benzene-d6) δ [ppm] = 4.85 (1H, s, [-N(C)(CH_3)(CH)(C)(CH_3)O-]), 3.64–3.21 (6H, m, [-N(CH_2) (CH_2)O(CH_2)(CH_3)]), 2.00 (3H, s, [-N(C)(CH_3)(CH)(C)(CH_3)O-]), 1.54 (3H, s, [-N(C)(CH_3)(CH)(C)(CH_3)O-]), 1.06 (3H, t, [-O(CH_2)(CH_3)]).

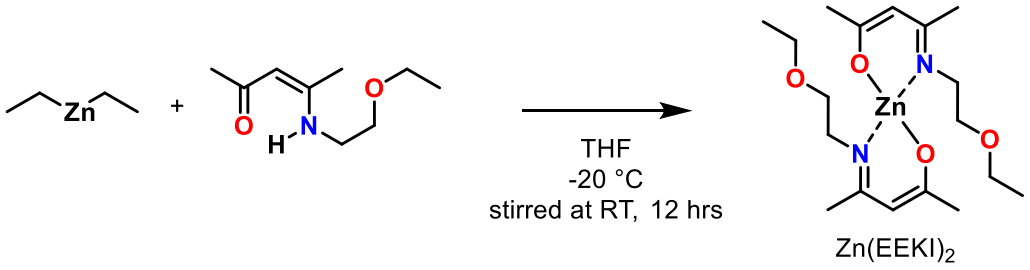

Scheme S2: Synthesis of $Zn(EEKI)_2$.

Ethyl(di(trimethylsilylamido))zinc, ZnEt(HMDS):

The synthesis of ZnEt(HDMS) was adapted from the work of Malik *et al.*[4] Diethyl zinc was dissolved in diethyl ether. After cooling the solution to -10 °C, an equimolar amount of hexamethyldisilazane was added slowly via syringe (Scheme S3). The reaction solution was allowed to warm to room temperature and then heated to reflux for 2 hours afterwards. The ether was distilled under reduced pressure, and afterwards the product was distilled as a clear liquid (yield: 80%).

^{1}H NMR (400 MHz, Benzene-d6) δ [ppm] = 0.09 (18H, s, [$((CH_3)_3Si)N$]), 0.12 (2H, q, [Zn(CH_2)(CH_3)]), 1.12 (3H, t, [Zn(CH_2)(CH_3)]).

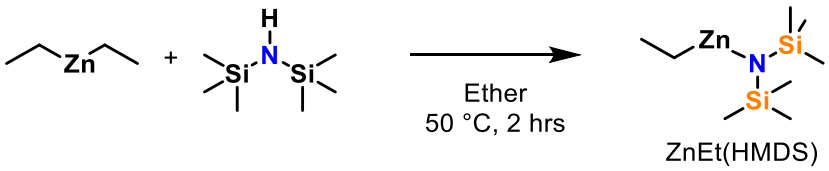

Scheme S3: Synthesis of ZnEt(HMDS)

ALD Process characteristics – *in-situ* spectroscopic ellipsometry

The GPC values for the different ALD processes studied have been measured using *in-situ* spectroscopic ellipsometry (isSE). The film thickness was calculated using a modified Cauchy model and plotted as a function of deposition time. Si(100) substrates were primed with 20 ALD cycles of the DEZ-water process to establish ZnO as the growth surface. During the temperature series, the reactor was given 30 minutes to reach thermal equilibrium. Then, 15 ALD cycles were performed for each parameter set, and the thickness change was recorded. Ignoring the first and last two cycles, the growth rate was determined through linear regression and converted to GPC, considering the specific deposition cycle duration, as exemplified for $Zn(DMP)_2$ in Figure S1.

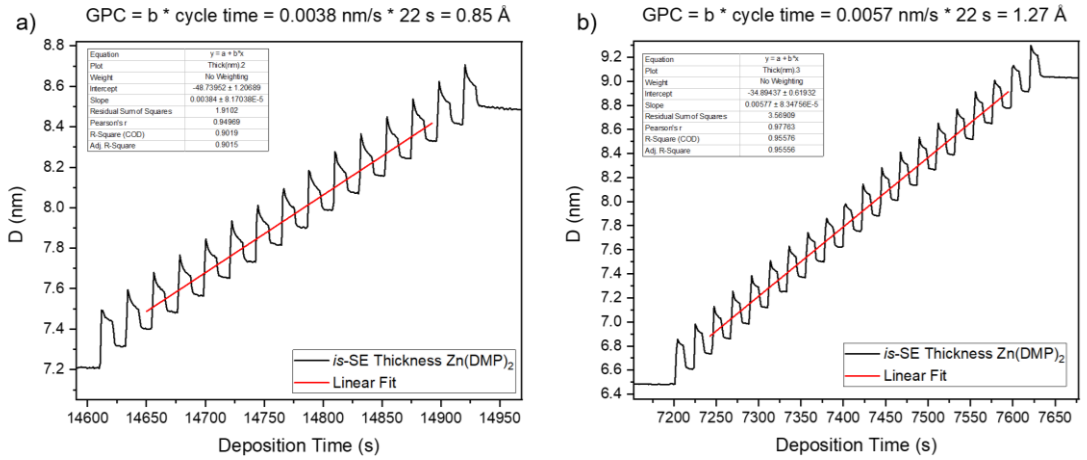

Figure S1: Exemplary isSE measurements demonstrating the temperature dependence of the $Zn(DMP)_2$ ZnO ALD process. a) shows isSE data collected for a deposition performed at 150 °C, b) isSE data collected for a deposition performed at 200 °C. Linear fits have been performed to extract the growth per cycle from the ellipsometry data. Thickness data (D) has been obtained by applying a modified Cauchy model to the measured ψ and Δ.

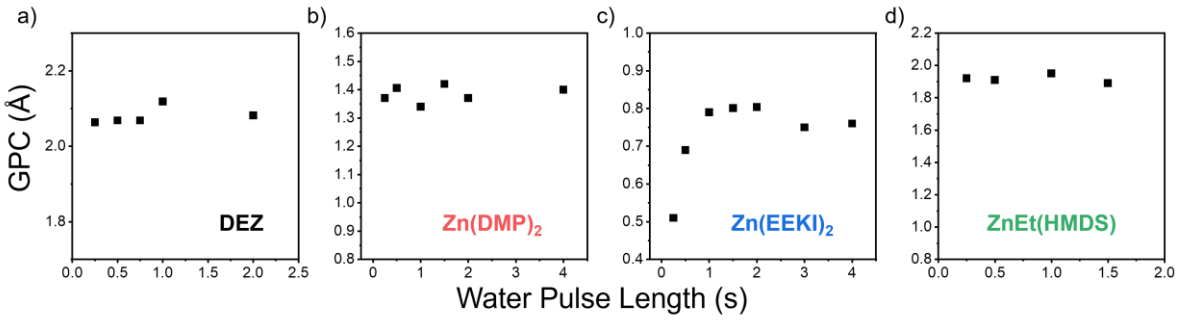

Figure S2: ALD saturation behavior for water co-reactant: growth per cycle versus H_2O pulse length for the three Zn precursors at 200 °C. a) DEZ pulse sequence 1-10-x-10, b) $Zn(DMP)_2$ pulse sequence 2-10-x-10, c) $Zn(EEKI)_2$ pulse sequence 2-10-x-10, and d) ZnEt(HMDS) pulse sequence 1-20-x-20.

XPS

XPS measurements were performed on thin films deposited by each of the four precursors. Peak fitting was undertaken for analysis and quantification. Below are the core-level spectra and corresponding fits for ZnO deposited by the four precursors at 200 °C. Very similar spectra were recorded for all samples and were fit using the same components. A charge correction was applied to the adventitious C 1s aliphatic component, setting it to 284.8 eV for all samples.

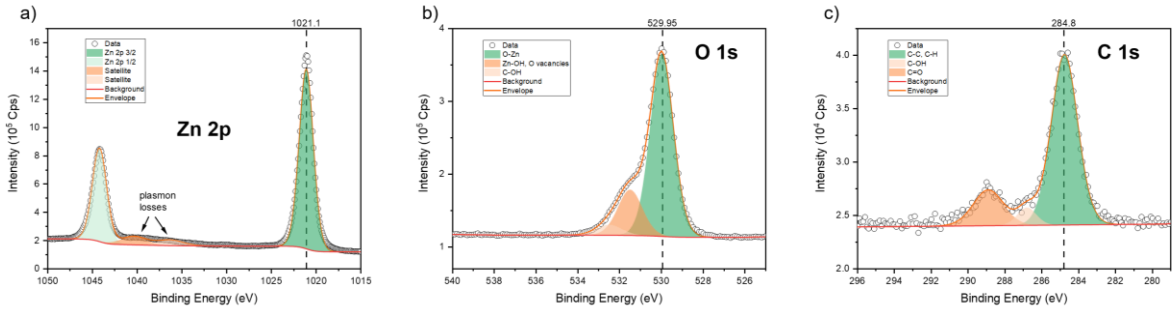

*Figure S3: As-introduced XPS core level spectra for a ZnO film deposited with **DEZ** and H_2O at 200°C. The a) Zn 2p, b) O 1s, c) C 1s core levels have been fitted with appropriate components.*

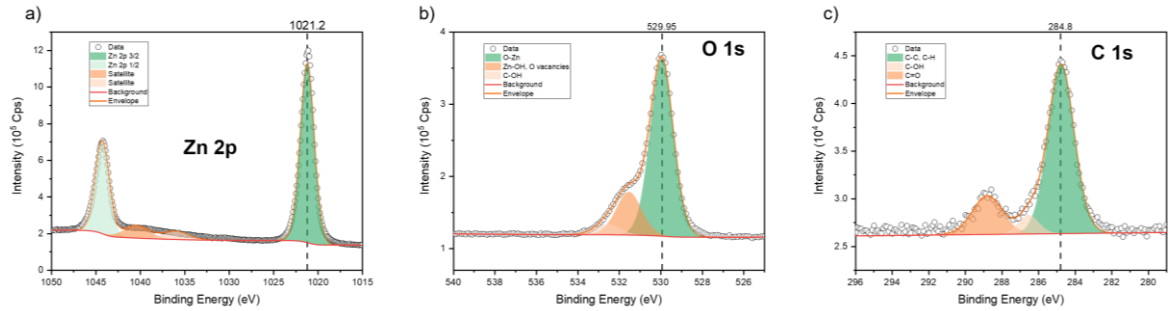

*Figure S4: As-introduced XPS core level spectra for a ZnO film deposited with **$Zn(DMP)_2$** and H_2O at 200°C. The a) Zn 2p, b) O 1s, c) C 1s core levels have been fitted with appropriate components.*

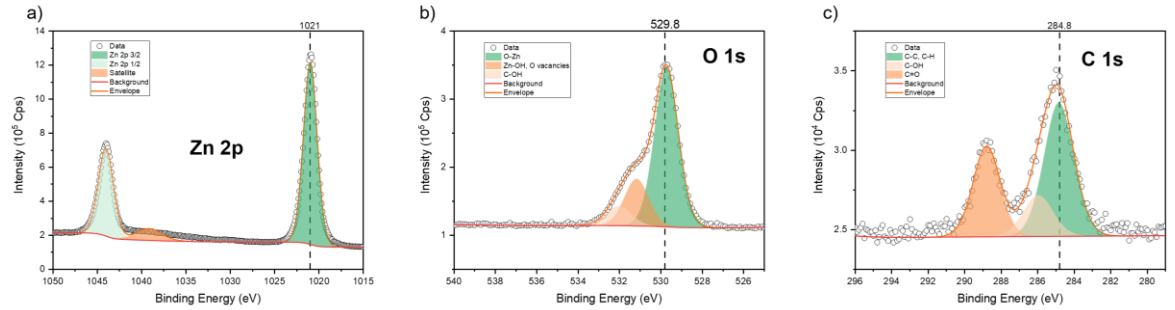

*Figure S5: As-introduced XPS core level spectra for a ZnO film deposited with **$Zn(EEKI)_2$** and H_2O at 200°C. The a) Zn 2p, b) O 1s, c) C 1s core levels have been fitted with appropriate components.*

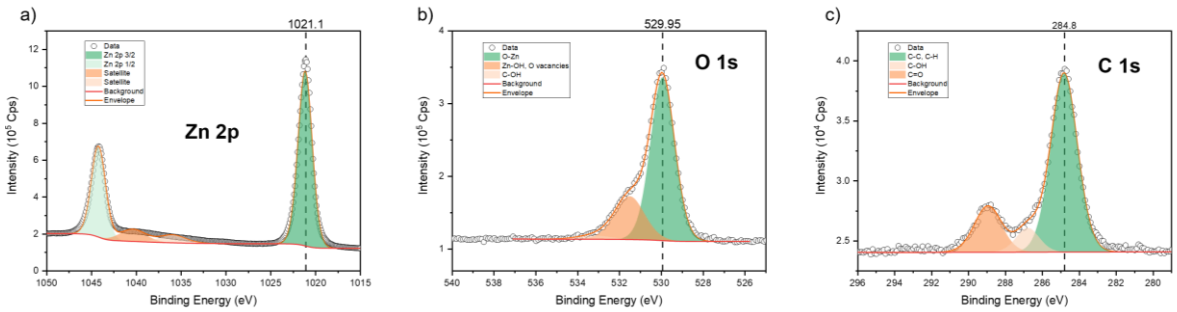

*Figure S6: As-introduced XPS core level spectra for a ZnO film deposited with **ZnEt(HMDS)** and H_2O at 200°C. The a) Zn 2p, b) O 1s, c) C 1s core levels have been fitted with appropriate components.*

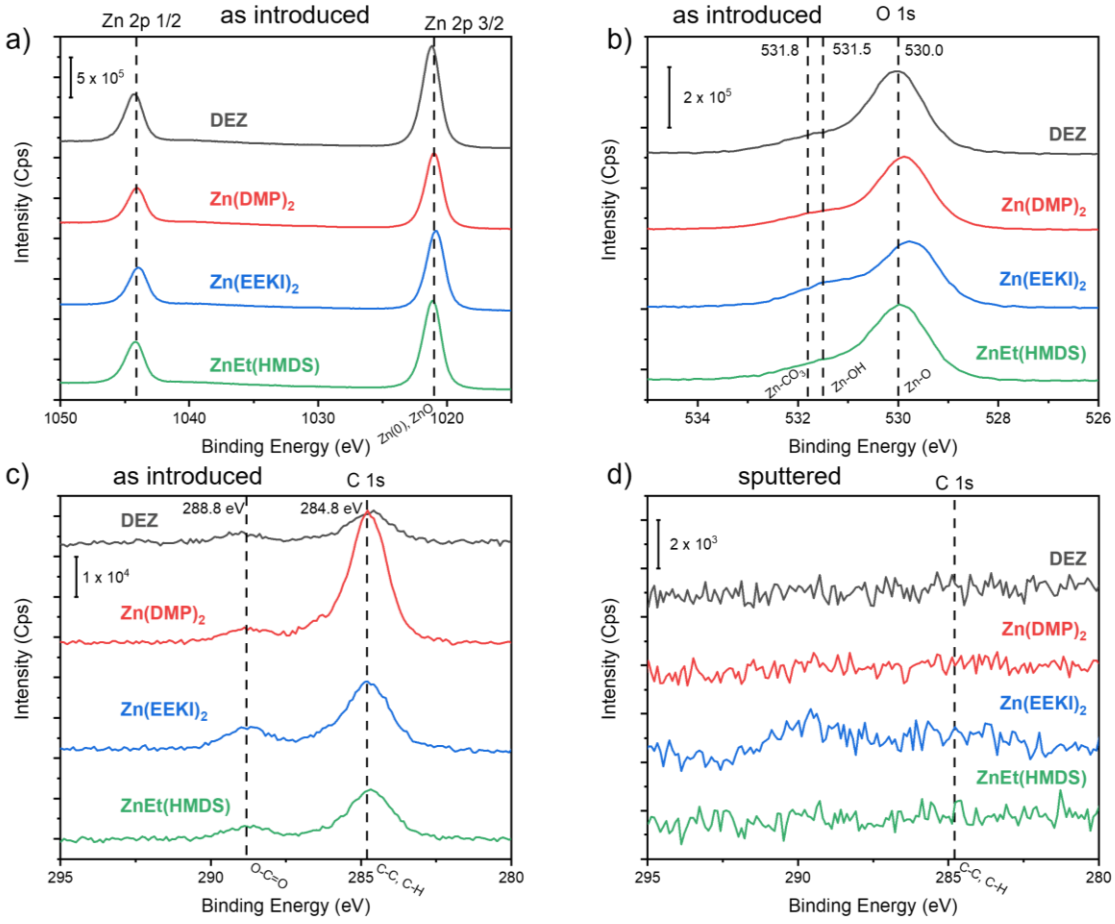

Figure S7: XPS core level spectra of a) sputtered Zn 2p, b) sputtered O 1s. Further, the as-introduced C 1s core level spectra c) are shown, used for charge referencing all recorded spectra, as well as d) the sputtered C 1s spectra. Spectra are stacked for the 4 different precursors used. Sputtering herein means 30 seconds at 2 keV.

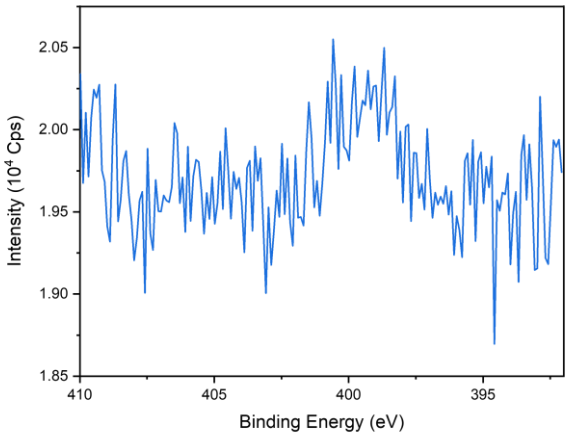

Figure S8: N 1s as-introduced XPS core level spectrum for a ZnO film deposited with $Zn(EEKI)_2$ and H_2O at 200°C. No nitrogen signals beyond the noise level were detected after sputtering.

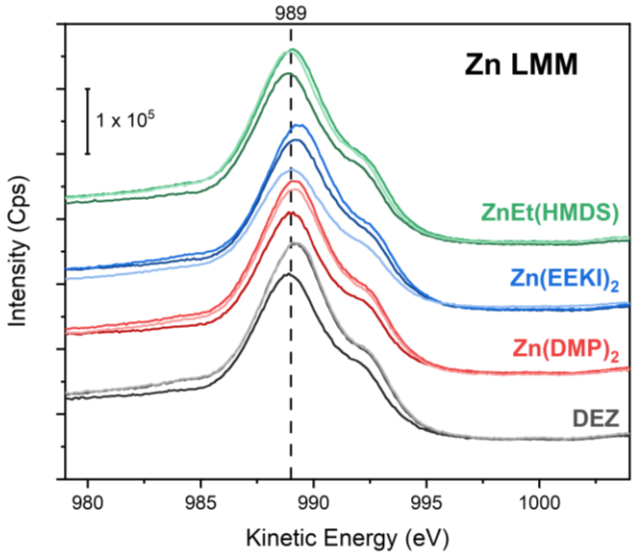

Figure S9: ZnLMM Auger peak spectra for a ZnO films deposited using DEZ, $Zn(DMP)_2$, $Zn(EEKI)_2$, and ZnEt(HMDS) with H_2O at 200°C.The as introduced and the spectra after the first two sputter steps are shown (dark to light).

Table S1: Modified Auger parameter (α) for ZnO thin films deposited using DEZ, $Zn(DMP)_2$, $Zn(EEKI)_2$, and ZnEt(HMDS) with H_2O at 200°C, alongside literature references. B.E. and K.E. values were for sputtered surfaces.

	B.E. Zn 2p 3/2 (eV)	K.E. Zn LMM (eV)	α (eV)
DEZ	1021.2	989.2	2010.4
$Zn(DMP)_2$	1021	989.2	2010.2
$Zn(EEKI)_2$	1020.9	989.3	2010.2
ZnEt(HMDS)	1021.1	989.1	2010.2
Literature ZnO	1021.9 1021.6	988.3 988.8	2010.2[5] 2010.4[6] 2010.2[7]
Literature Zn(0)			2013.8[7]

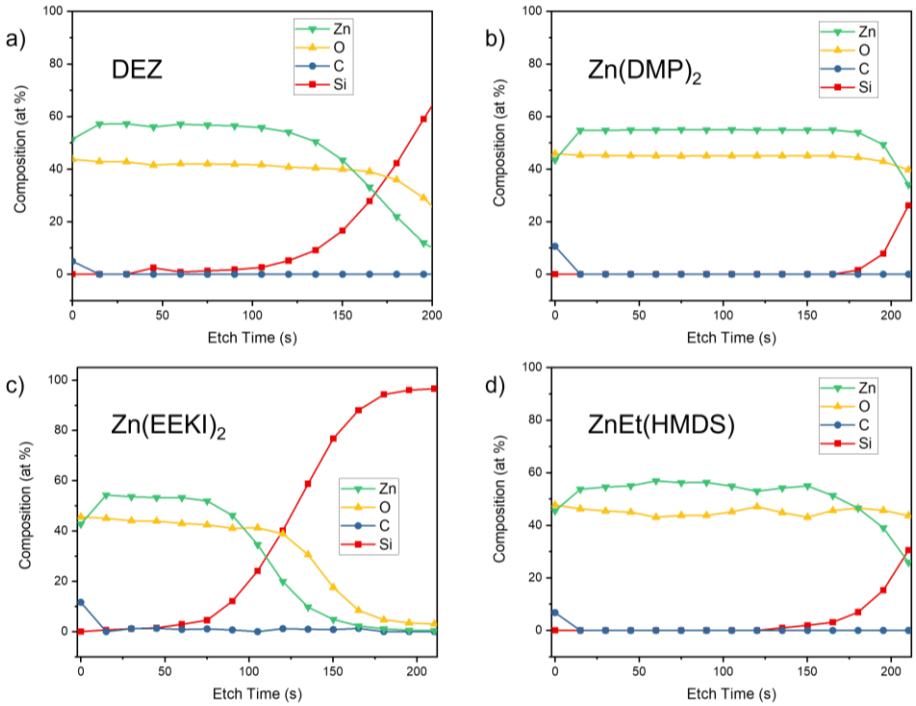

Figure S10: XPS composition depth profiles of ZnO films deposited using a) DEZ, b) $Zn(DMP)_2$, c) $Zn(EEKI)_2$, and d) ZnEt(HMDS). Profiles were extracted from XPS data by integrating the peak areas of the respective components. For Zn and Si, the 2p 3/2 component was used for the integration.

UV-Vis Spectra

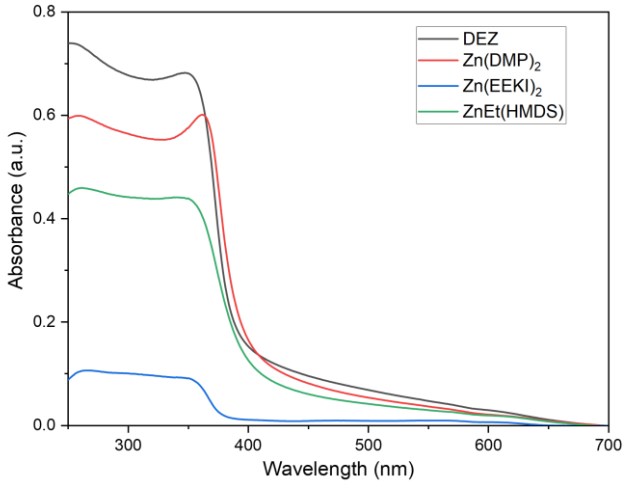

Figure S11: UV/Vis absorption spectra of the ZnO thin films deposited from the four investigated precursors onto quartz substrates. The significant difference in the absorbance intensity of the $Zn(EEKI)_2$ film results from the notably thinner film that was formed because of the lower growth rate with this precursor.

XRD and UV-Vis

Table S2: XRD full-width half-maxima for the (200) reflex of the ZnO thin films deposited using the four different precursors. Peaks were fitted with a Gaussian peak shape. XRR fitted material densities and bandgap values from UV-Vis measurements.

	DEZ	$Zn(DMP)_2$	$Zn(EEKI)_2$	ZnEt(HMDS)	Literature
ZnO (200) FWHM / °	0.43	0.44	0.71	0.30	
Band gap / eV	3.24	3.20	3.32	3.19	3.37[8]

Literature

1 L. Mai, F. Mitschker, C. Bock, A. Niesen, E. Ciftyurek, D. Rogalla, J. Mickler, M. Erig, Z. Li, P. Awakowicz, K. Schierbaum and A. Devi, *Small*, 2020, **16**, 1907506.

2 L. Mai, D. Zanders, E. Subaşı, E. Ciftyurek, C. Hoppe, D. Rogalla, W. Gilbert, T. D. L. Arcos, K. Schierbaum, G. Grundmeier, C. Bock and A. Devi, *ACS Appl. Mater. Interfaces*, 2019, **11**, 3169–3180.

3 R. O' Donoghue, D. Peeters, D. Rogalla, H.-W. Becker, J. Rechmann, S. Henke, M. Winter and A. Devi, *Dalton Trans.*, 2016, **45**, 19012–19023.

4 M. A. Malik and P. O'Brien, *Polyhedron*, 1997, **16**, 3593–3599.

5 C. Morales, A. Black, F. J. Urbanos, D. Granados, J. Méndez, A. Del Campo, F. Yubero and L. Soriano, *Adv. Mater. Interfaces*, 2019, **6**, 1801689.

6 S. Bera, S. Dhara, S. Velmurugan and A. K. Tyagi, *Int. J. Spectrosc.*, 2012, **2012**, 1–4.

7 L. S. Dake, D. R. Baer and J. M. Zachara, *Surf. Interface Anal.*, 1989, **14**, 71–75.

8 A. Adhikari, E. Przezdziecka, S. Mishra, P. Sybilski, J. Sajkowski and E. Guziewicz, *Phys. Status Solidi A*, 2021, **218**, 2000669.